International Journal of Bioelectromagnetism *www.ijbem.org*
Vol. 22, No. 1, pp. 25 - 36, 2020

Impedimetric Sensor Using Electric Relaxation

Uwe Pliquett[1], Danny Echtermeyer[1], Katharina Schieke[1], Andreas Sachse[2]
[1]*Institut für Bioprozess- und Analysenmesstechnik, Heilbad Heiligenstadt, Germany*
[2] *Micro-Hybrid Electronic GmbH, Hermsdorf, Germany*

Correspondence: Uwe Pliquett, Institut für Bioprozess- und Analysenmeßtechnik e.V.
Heilbad Heiligenstadt, Rosenhof 1, D-37308, Germany
uwe.pliquett@iba-heiligenstadt.de

Abstract. The electrical characterization of single cells, cell suspensions, and tissue but also functionalized surfaces for sensing applications based on impedance spectroscopy is widely deployed and well accepted. While most applications use step sinus excitation for sweeping through the frequency range of interest, methods in the time domain with broad bandwidth excitation signals like multi sinus or chirp become increasingly prominent. The use of transient excitation like Dirac function or step function exhibits advantages for low energy applications with low hardware requirements. Especially the electric relaxation of a system after the application of a voltage or current step is comparatively simple to monitor while the generation of the stimulus does not need extensive hardware. Established models for biological objects but also for electrodes and functionalized surfaces can be calculated directly in the time domain without transformation into the frequency domain. As an example, we present an impedimetric sensor for detecting the growth of bacterial biofilms.

Keywords: Biosensor, Aptamer, impedance, electric relaxation, step response

1. Introduction

Electrical relaxation is the time course of a physical quantity like voltage or current changing from one state to another as a result of a transient excitation (Cole, 1955). From the theoretical point of view, the Dirac function (impulse) is the ideal excitation function but lacks practicability. It is impossible to generate a Dirac function, but even the creation of useful impulses for measurement purpose need sophisticated hardware. Much simpler is the switch from one voltage or current level to another, which is not an ideal step as well but can be realized with short switching time and good stability after the step using digital techniques. For less demanding applications with an upper frequency below 1 MHz, the direct output of many digital-analog-converters (DAC) is sufficient.

The accessible frequency band is limited by the rise time of the step function, the quality of the step function (e.g., the appearance of overshoot), and the duration of the stimulation after the step occurred. Given a high-quality stimulus with no overshoot, fast rise time, and a stable level after the step makes the tracing of the stimulus unnecessary, at least for low precision requirements. Additionally, to the signal quality, the upper frequency is limited by half of the speed of the analog-digital converter (ADC). A problem arises for economic, stand-alone instrumentation with broad bandwidth with respect to the data volume. For instance, if the bandwidth is five decades from 0.5 Hz to 50 kHz, 100.000 time instants are necessary (100 kS/s for 0.5 s). This is not a problem when using standard equipment like digital oscilloscopes but is not compatible with microcontroller based instrumentation with, for instance, only 2 kB memory (Gansauge, Zaikou, Schroeder, Schemberg, & Pliquett). A practical solution is the non-equidistant sampling with fast integration and conversion immediately after the step occurred and slowing down with time. A problem is the aliasing effect which becomes extremely prominent with long times between time instants (e.g., 100 ms) and measurement noise with frequency compounds up to the

upper frequency limit of the instrument (e.g., 50 kHz). To avoid this problem, partial integration of the step response is used, which acts like an adaptive anti-aliasing filter (Horowitz & Hill, 1980).

Because the sample times are exactly known, a complete reconstruction of the step response is possible. Since typical models for biologic objects do not involve resonance points and no inductance (Grimnes & Martinsen, 2014), the step answer to a potential step is at first glance a sum of decaying exponentials. Models typically involve one or two polarization processes. If the data cannot be fitted with one or two exponentials, it is advisable to introduce constant phase elements (e.g., Q_m in Fig. 1), which yield in time domain either a distribution of relaxation times (Cole-model) (BioLogic, 2017) or an exponential function with fractal exponent. Other models exist but are not in use for modeling results from bioimpedance measurements. Capacities in cell-based materials are mostly due to cell membranes, while resistive parts arise from electrolytes in and outside the cells (Schwan, 1957).

If electrodes are involved. and a voltage step is applied, a further decay of the current with $t^{-\alpha}$ dependence (t^{α} when the current step applied) on time is evident. This is due to material diffusion and is modeled by a constant phase element (CPE) (Sadkowski, 2000), an apparent capacitor depending on α and having the unit F/s^{1-a}. Ideally, when α=0.5, the phase of this element is constant at 45° (Warburg behavior). Electrodes are often modeled using a modified Randles circuit (the green portion in Fig. 1), which involves the charge transfer resistance R_{ct} and a double layer capacitance C_{dl}. The material diffusion to and away from the electrode is modeled as the Warburg element in series to the R_{ct}. Theoretically, R_{ct} and C should form an ideal RC-element at high frequency where the Warburg impedance does not matter due to the comparatively slow diffusion. However, in practice, data are much better approximated using CPE-behavior ($C_{cl} \rightarrow Q_{cl}$).

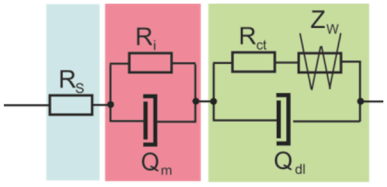

Figure 1. *Hypothetical equivalent circuit for an electrode with an attached biologic system. Rs is the resistance of the bulk electrolyte (saline), and R_iQ_m is the resistance of intracellular electrolytes and the membrane capacitance. R_{ct}, Z_W and Q_{dl} are the elements of the modified Randles Circuit as a model for electrodes in contact with electrolytes.*

The processing of the relaxation curve aims in fitting the elements of the equivalent circuit and further the interpretation of all elements on the cellular and molecular level. Here, the basic features of the instrumentation, together with fitting of the data to an equivalent circuit, are shown.

2. Material and Methods

2.1 Electrode array

The sensor arrangement (Fig. 2) was formed on a corundum ceramic base with a thickness of 0.63 mm. The gold working electrodes, each with an area of 0.30 cm², were applied to this surface. The sensor forms an arrangement of eight independently controllable electrodes. It was developed and produced by Micro-Hybrid Electronic GmbH, Hermsdof, Germany.

The electrode array was first placed in a special incubation chamber in which each individual electrode could be treated separately. It was washed with 80% EtOH and then rinsed with distilled water. For further cleaning, a basic piranha solution (H_2O:NH_3:H_2O_2 = 5:1:1 v/v) was applied for 10 minutes, then rinsed several times with distilled water and finally air-dried.

For measurement purposes, the electrode was placed in the measuring chamber, where all the individual electrodes shared the Ag/AgCl reference electrode made of chlorinated silver mesh, and the counter electrode made of stainless steel. The active area of the working electrode within the measuring chamber was 0.25 cm². The active area of the counter electrode was 2.47 cm². The solutions (medium and buffer) were pumped through the chamber using a peristaltic pump.

Figure 2. *Electrode array (Micro-Hybrid Electronic GmbH, Hermsdof, Germany) as substrate for biofilm growth. Each individual gold electrode has a surface area of 0.40 cm².*

2.2 Biofilm growth

The *E. coli* K12 bacterial strain was cultured in Erlenmeyer flasks using standard Luria Bertani medium (10 g/l tryptone, 20 g/l yeast extract, and 5 g/l NaCl in deionized water) at 37°C overnight in a laboratory shaker. The cells were then washed with LB medium, and the density was determined by counting the labeled cells under the microscope. For further experiments, the cell culture was diluted to 10^6 cells/ml and 10^7 cells/ml, respectively, with LB medium. Both dilutions were applied to each two electrodes so that four electrodes were used for the biofilm growth, and four electrodes served as a blind reference. After 48 hours of incubation at 37°C in the incubation chamber, the electrode array was placed in the measuring chamber and washed with fresh LB medium. The biofilm growth was carried out in an incubator at 37°C.

The impedance measurements were carried out in the measuring chamber immediately after the electrode array had been transferred from the incubation chamber, after 2 h of biofilm growth and again after 24 h of biofilm growth. We used 140 mM PBS (phosphate-buffered saline) for washing the electrode array and measuring buffer (140 mM PBS with 2 mM ferric / ferrocyanide redox pair) for the impedance measurements.

2.3 Electrical measurement system

Because electrical characterization was done in the time domain on the basis of current relaxation (Pliquett, 2018) to a voltage step, the timing of the stimulus and the sampling regime was determined rather than the frequency vector for impedance measurement.

The lowest assessable frequency is limited by the length of the signal after the step occurred. In the example shown here, it is 0.5 Hz with a signal length of 1 s. The upper limit arises from sampling speed, which is 400 kHz by using the ADuC841-controller (Analog Devices, Norwood, MA) but can be easily extended by using an external ADC. In the example shown here, an upper frequency of 10 kHz was specified, which even allowed oversampling for noise reduction.

The schematic of the instrument is shown in Fig. 3. The microcontroller ADuC841 (Analog Devices, Norwood, MA) generates the stimulus, schedules the integration and reset of the integrator, samples the integrated curve, and digitizes it. The partial integration of the current instead of direct sampling provides a simple way for the implementation of an adaptive anti-aliasing filter.

The DAC of the microcontroller provides the stimulus, here a 32 mV voltage step. The sampling regime depends on the material under test (MUT), especially on the relaxation times expected for the material.

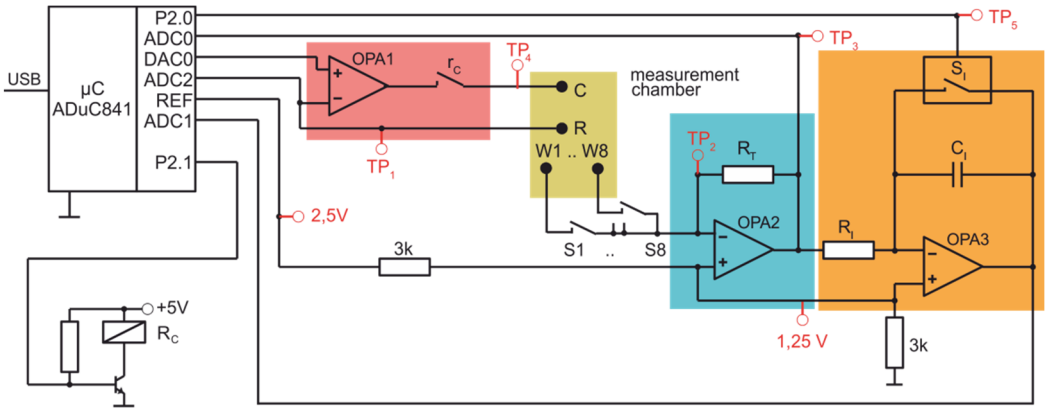

Figure 3. *Schematic of the instrument. The microcontroller generates the stimulus using the internal digital-analog-converter, which drives the counter electrode C of the measurement chamber. The voltage at the reference electrode R is fed back to the inverting input of OPA1 for controlling the voltage between reference and working electrode W. The current through the working electrode is converted to a voltage by the transimpedance (OPA2/R_T) and fed through the Resistor R_I into the resettable integrator (OPA3/C_I/S_I) Both, the voltage at the reference electrode and the output of the integrator is monitored using the analog-digital-converters (ADC) of the microcontroller. For testing the resting potential, which appears at R when the current through W is zero, a relay (R_C) disconnects the counter electrode, which is more precise than setting DAC0 to the reference voltage of the analog part (1.25V).*

2.4 Data acquisition

The timing of the stimulus, integrator start and reset and also the data acquisition is maintained by the firmware of the microcontroller. Because only low-frequency behavior below 10 kHz was required, all sampling was done with 16x oversampling, which greatly reduces the instrument noise. Moreover, synchronization with the 50 Hz from the power line could reduce the influence from the crosstalk (Fig. 4). This was extraordinarily important because tubing and relatively long wiring catch up considerable noise.

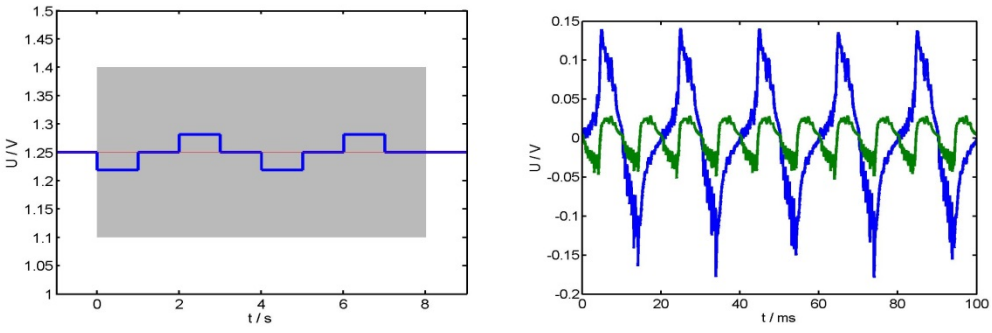

A B

Figure 4. *(A) Excitation signal for measurement from 0.5 Hz up to 100 kHz. (B) The blue line shows a 50 Hz noise catched by the instrument when long wires without any shielding were used while the green line results after summing with the 180°-shifted signal.*

The first four steps (Fig. 4A, -1,+1,+1,-1) are all precisely within a 20 ms-grid (50 Hz noise from a power line) while the next four steps have the same time schedule but with a 10 ms delay to the first group. By adding the step responses from the +1 and the -1-steps with the inverted polarity of the -1-steps, asymmetry, and non-linearity of the instrumentation were depressed. 50 Hz influence was reduced by more than 60 dB for all parts of the signal lasting longer than 20 ms by integrating over multiples of 20 ms for each time instant. The 10 ms delay between the step groups aimed in a depression of 50 Hz-noise until 20 ms after the step occurred. Depression of the 50 Hz for times shorter than 20 ms is shown in Fig. 4B. In the ideal case of a pure sine wave without harmonics, noise extinction by adding the signal with 0° and 180° phase shift would be effective. However, due to its asymmetry and occurring harmonics, only partial cancellation was achieved (green line in Fig. 4B). Comparing the 50 Hz-content of the first four step responses and this after adding the second four-step responses showed a depression of the 50 Hz by more than 30 dB, which is much better than the example sown in Fig. 4B.

The sampling between the steps includes the reset of the integrator (discharge of C_I in Fig. 3), integration of the current for a predetermined time (Fig. 4, blue line), and analog-digital conversion.

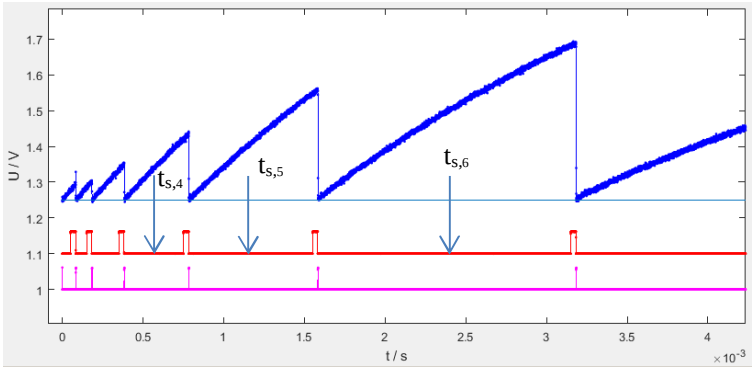

Figure 5. *The signal at the output of the integrator (blue line ADC1), the period of AD-conversion (orange line, internal signal) and the reset at S_I (magenta line, P2.0. While a 50 Hz synchronization is not possible for the time range 0..20 ms, further integration periods are always multiples of 20 ms. The cyan line indicated the analog reference of the instrument at 1.25 V ($U_{ref}/2$). As an example, the arrows indicate the time instants 4..6 used for further processing.*

The sampling regime started with a fast period using instants of time t_s with corresponding integration times t_i as listed in table 1. It should be noted that the time instants t_s do not equal the time of AD-conversion, but they are between them (see arrows in Fig. 5). In this sense, half of the sampled value is proportional to the mean value over the integration time. Practically, the error due to current changes during the integration interval is negligible with the settings used here. Since only the mean value of the integration period is used, any frequency above $1/t_i$ is suppressed, which is - due to increasing t_i - an adaptive anti-aliasing filter.

In order to ensure minimal signal distortion, the integrator was activated immediately before the step occurred. Therefore, the first integration interval started before the step and ended immediately after.

Table 1. *Sampling time instants and integration times for the first 10 ms-interval. The integration intervals are always between the instants of the sampling time*

t_s / ms	0.033	0.126	0.277	0.576	1.17	2.24	4.77	8.18
t_i / ms	0.065	0.082	0.18	0.38	0.78	1.58	3.16	3.5

After the last time instant within the first 10 ms, integration continued and stopped at 10 ms. Subsequently, integration over 20 ms intervals was repeated 48 times. A necessary small gap of 6 µs for reset was corrected in further processing. The further acquisition regime started with the memorizing the first 20 ms- sample (integration from 10 ms – 30 ms) followed by the sum of the two next samples, than summarizing four samples and so on until 0.98 s was reached (tab.2). The last interval was not complete (35x instead of 64x) in order to have time for the preparation of the next step and to synchronize to 1 s.

Table 2. *Sampling time instants and integration times for the first 20 ms-interval. The integration intervals are always between the instants of the sampling time.*

t_s / ms	20	50	110	230	470	805
t_i / ms	20	40	80	160	320	350

The data until 10 ms is stored internally and transmitted to the host computer within the first 20 ms integration interval. All other data are transmitted immediately after the last sample of the integration interval was summed.

During a measurement cycle, first the relay R_G is open in order to equilibrate the electrode-electrolyte interface and checking the resting potential for a reasonable value. This was used for presetting the offset of the measurement in order to start always with the resting potential. The second step adjusts the reference voltage to a value where the current through the MUT is zero (resting potential). This is done by reading the voltage at TP3/ADC0 and the successive adjustment of the voltage offset. As soon as the electrode behaves stable, the cycle with eight single steps is initiated, and the data transferred to the host

computer. At the end of the measurement, the relay switches off to avoid electrode reactions due to a drift of the resting potential.

2.5 Data processing

The first step is the calibration of all ADC-offsets with the values obtained during the setup phase of the instrument turning on the supply voltage. The true current through the MUT is calculated from the data using the transfer function of the measurement chain, especially the values of R_T, R_I, and C_I.

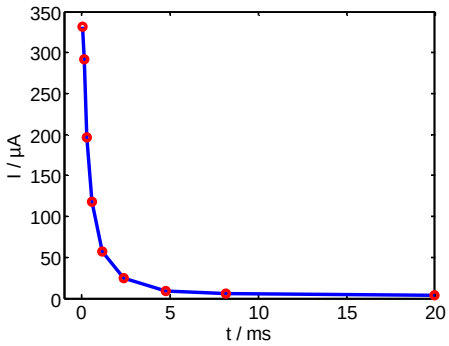

Figure 6. *Example of the first 20 ms of a step response (i(t) through the MUT) to a potentiostatic step after 48h of incubation with E.coli gold electrode. The red dots are the time instants.*

The typical model for electrodes covered with layers like biofilm is shown in fig.1. However, testing the significance of the model parameter, R_i, and Q_m, the parameters modeling the cells have not been significant. Therefore, the model was reduced to the modified Randles circuit, where the double layer capacitance is replaced by a constant phase element (CPE), accounting for distribution in relaxation behavior on the molecular level. Thus, the current response due to a voltage step is not purely exponential but somehow between exponential and polynomial.

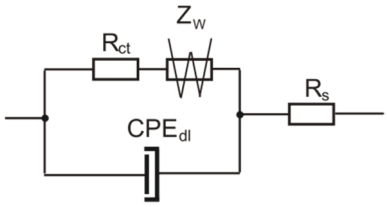

Figure 7. *Modified Randles circuit accounting for the electrical behavior of a bacterial biofilm covered gold electrode. R_{ct} is the charge transfer resistance accounting for the electron transfer at the electrode, Z_W is the Warburg impedance, depending on the mass transport within the Gouy-Chapman-layer due to diffusion, CPL_{dl} is the constant phase element which is formed by the double layer at the electrode and R_s is the resistance of the electrolyte (saline).*

Two elements (CPE, Z_W) in the electrical circuit shown in Fig. 6 are constant phase elements, which are non-ideal elements in terms of RLC because they depend on frequency.

$$Z_W = \frac{A_W}{\sqrt{s}} \qquad Z_{CPE_{dl}} = \frac{1}{Q_{dl}s^{\alpha}} \tag{1}$$

where s is the complex frequency ($s = \sigma + j\omega$, σ reciprocal of a time constant, ω the angular frequency $\omega = 2\pi f$, j imaginary unit $j = \sqrt{-1}$). A_W is the Warburg coefficient (unit $\Omega s^{-0.5}$), and Q_{dl} is the frequency-dependent double layer capacity with the unit $Fs^{1-\alpha}$. Q_{dl} becomes a pure capacitor for $\alpha = 1$ but behaves resistive for $\alpha = 0$.

The admittance of the circuit shown in Fig.6 is

$$Y_R = \frac{R_{ct}Qs^{\alpha} + A_W Qs^{\alpha-0.5} + 1}{R_{ct} + R_s + A_W s^{-0.5} + R_s R_{ct} Qs^{\alpha} + R_s A_W Qs^{\alpha-0.5}} \tag{2}$$

The attempt to directly transform this expression into time domain did not yield a result by using inverse Laplace transformation aided either by an online integrator (*https://www.integralrechner.de/*) or a correspondence table providing solutions for fractional exponents (Monje, Chen, Vinagre, Xue, &

Feliu, 2010). To overcome this problem, an algorithm was developed which first calculates a model where the solution is known. In a second step, the conductance of this model is converted to the conductance of the modified Randles circuit.

2.6 Calculation of the elements of Randles circuit from current relaxation after the voltage step

Modeling electrical response yields an equivalent electrical circuit, such as the modified Randles circuit shown in Fig. 6. The advantage of this circuit is that each element has a physical meaning. The disadvantage is that it cannot directly be transformed in the time domain. For other circuits, giving exactly the same response, a solution exists. Therefore, the elements represent a mixture of different physical behavior, which makes it difficult to find, for instance, the charge transfer resistance R_{ct}. To overcome this problem, we divide the calculation of the elements of the Randles circuit into two steps:

(1) Calculation of the elements of a circuit with the same electrical response
(2) Conversion of these elements into the elements of Randles circuit

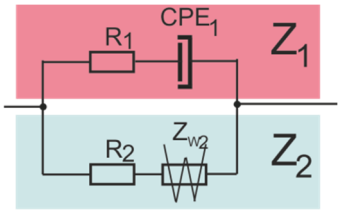

Figure 8. *Equivalent circuit with the same impedance as the modified Randles circuit. Z_1 and Z_2 stay for the impedances of both branches. Although Z_1 is dominated by the double layer and the behavior of the biofilm and Z_2 represents in a first glance the diffusional mass transport and the resistance of the saline, all elements are interconnected in a complicated manner.*

The expression for the admittance of the circuit in Fig. 7 is rather simple due to two parallel combinations. The impedances Z_1 and Z_2 are

$$Z_1 = R_1 + \frac{1}{Q_1 s^{ß}} \qquad Z_2 = R_2 + \frac{A_{W2}}{\sqrt{s}} \tag{3}$$

The total admittance of the parallel combination (fig.7) is

$$Y_p = \frac{1}{R_1 + \frac{1}{Q_1 s^{ß}}} + \frac{1}{R_2 + \frac{A_{W2}}{\sqrt{s}}} \tag{4}$$

This yields an expression where both summands can be transformed separately, and their step response i_{Y_P} added (fig.8) as partial currents i_{Z_1} and i_{Z_2}.

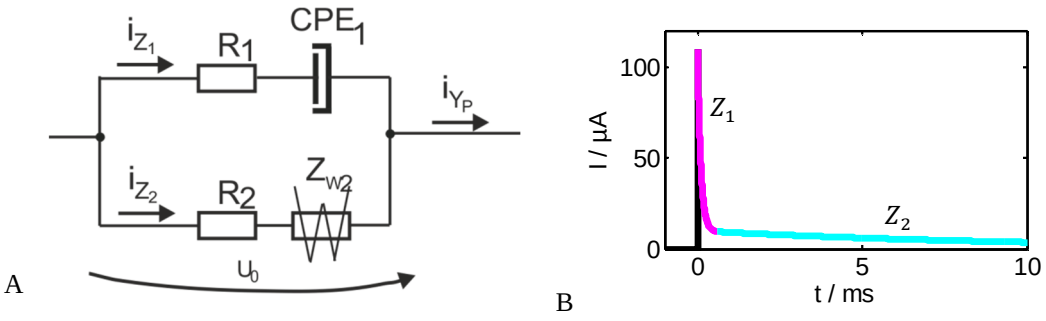

Figure 9. *(A) Parallel equivalent circuit with admittance Yp and the partial currents i_{Z_1} and i_{Z_2}, which yields the total current i_{Y_P} as a response to a voltage step of U_0.(B)Current response indicating the time where Z_1 and Z_2 dominate the response.*

Immediately after the voltage step (high frequency), the electrolyte resistance R_S overwhelms the electrical response while at a later time (low frequency) the serial combination of a Warburg element Z_W with the electrolyte resistance dominates the electrical properties.

The fitting starts with the low-frequency part, i.e., the current due to diffusion in the Gouy-Chapman-layer yields a contribution that can be extrapolated to the time t0 when the step was applied and subtracted from the total current. According to Eq. 4, the admittance of this branch is

$$Y_2 = \frac{1}{A_{W2}s^{-0.5} + R_2} = \frac{1}{R_2}\frac{1}{\frac{A_{W2}}{R_2}s^{-0.5} + 1} \tag{5}$$

The multiplication of the Laplace transformed voltage step (U_0/s) yields the current response in the frequency domain:

$$I_2(s) = \frac{U_0}{R_2}\frac{1}{s\left(\frac{A_{W2}}{R_2}s^{-0.5} + 1\right)} = \frac{U_0}{R_2}\frac{1}{s(as^{-0.5} + 1)} = \frac{U_0}{R_2}\frac{s^{0.5}}{s(a + s^{0.5})} \tag{6}$$

$\frac{s^{0.5}}{s(s^{0.5}+a)}$ corresponds to $\mathfrak{E}_{0.5,1}(-at^{0.5})$ in the time domain (Monje et al., 2010), where $\mathfrak{E}_{\alpha,\beta}(z) = \sum_{k=0}^{\infty}\frac{z^k}{\Gamma(\alpha k + \beta)}$ is the Mittag-Leffler-function (Haubold, Mathai, & Saxena, 2011). The Γ stays for the gamma-function. Therefore, the current in time-domain is:

$$i_2(t) = \frac{U_0}{R_2}\mathfrak{E}_{0.5,1}\left(-\frac{A_{W2}}{R_2}\sqrt{t}\right) \tag{7}$$

After subtracting $i_2(t)$ from the total current, $i_1(t)$ remains. It can be derived similarly to $i_2(t)$. The conductance

$$Y_1 = \frac{1}{R_1 + \frac{1}{Q_1 s^{ß}}} = \frac{1}{R_1 Q_1}\frac{Q_1 s^{ß}}{s^{ß} + \frac{1}{R_1 Q_1}} = \frac{1}{R_1}\frac{s^{ß}}{s^{ß} + \frac{1}{\tau_1}} \quad ; \quad \tau = R_1 Q_1 \tag{8}$$

multiplied with the transformed step function yields the current

$$I(s) = \frac{U_0}{R}\frac{s^{ß}}{s\left(s^{ß} + \frac{1}{\tau}\right)} \tag{9}$$

The correspondence table for $\frac{s^{\alpha}}{s(s^{\alpha}+a)}$ yields $\mathfrak{E}_{\alpha,1}(-at^{\alpha})$ and therefore the partial current

$$i_1(t) = \frac{U_0}{R_1}\mathfrak{E}_{ß,1}\left(-\frac{t^{ß}}{R_1 Q_1}\right) \tag{10}$$

After fitting of $i_1(t)$, all elements of the circuit in Fig. 7 are determined. Combining Eq. 7 and Eq. 10 yields the total current through the parallel combination of a Warburg and a CPE-branch.

$$i_p(t) = \frac{U_0}{R_1}\mathfrak{E}_{ß,ß}\left(-\frac{t^{ß}}{R_1 Q_1}\right) + \frac{U_0}{R_2}\mathfrak{E}_{0.5}\left(-\frac{A_{W2}}{R_2}\sqrt{t}\right) \tag{11}$$

The calculation of the Randles circuit from the known elements of the parallel circuit is done by comparison of their admittances and solving a system of equations. Using Eq. 2

$$Y_R = \frac{R_{ct}Qs^{\alpha} + A_W Qs^{\alpha-0.5} + 1}{R_{ct} + R_s + A_W s^{-0.5} + R_s R_{ct} Qs^{\alpha} + R_s A_W Qs^{\alpha-0.5}}$$

and the slightly manipulated Eq. 4

$$Y_P = \frac{(R_1 + R_2)Q_1 s^{ß} + A_{W2} Q_1 s^{ß-0.5} + 1}{R_2 + A_{W2} s^{-0.5} + R_1 R_2 Q_1 s^{ß} + R_1 A_{W2} Q_1 s^{ß-0.5}}$$

yields $A_W = A_{W2}$. The relation of the resistors at dc (s = 0) is $R_2 = R_{ct} + R_s$ while at infinite frequency, s→∞ $R_s = \frac{R_1 R_2}{R_1 + R_2}$. Therefore, $R_{ct} = \frac{R_2^2}{R_1 + R_2}$. A further comparison of coefficients is not possible because $a \neq ß$.

A possible solution, which will be shown here, is omitting the already known Warburg element at high frequency, which simplifies the equation for Randles circuit. Therefore, a significance test for the influence of the Warburg element at high frequency would be required.

The simplified circuit without the Warburg-element, together with the derivation of the admittance is shown in Fig. 9.

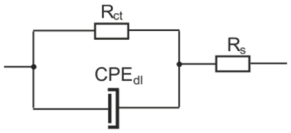

Figure 10. *Serial circuit (Modified Randles circuit) without Warburg element*

The impedance is

$$Z_S = \frac{\frac{R_{ct}}{Q_{dl}s^{\alpha}}}{R_{ct} + \frac{1}{Q_{dl}s^{\alpha}}} + R_s = \frac{R_{ct} + R_s(1 + R_{ct}Q_{dl}s^{\alpha})}{1 + R_{ct}Q_{dl}s^{\alpha}} \tag{12}$$

The reciprocal of Eq. 12 is the admittance

$$Y_S = \frac{1 + R_{ct}Q_{dl}s^{\alpha}}{R_s + R_{ct} + R_s R_{ct} Q_{dl} s^{\alpha}} \tag{13}$$

The Warburg coefficient A_W and the resistors R_{ct} and R_s are already determined. For calculation of Q_{dl} and α the admittance at two frequencies, s_1 and s_2, is required. Inserting it into the admittance for the yields

$$Y_1 = \frac{1 + R_{ct}Q_{dl}s_1^{\alpha}}{R_s + R_{ct} + R_s R_{ct} Q_{dl} s_1^{\alpha}} \quad \text{and} \quad Y_2 = \frac{1 + R_{ct}Q_{dl}s_2^{\alpha}}{R_s + R_{ct} + R_s R_{ct} Q_{dl} s_2^{\alpha}}.$$

Solving for $s^{ß}$ gives:

$$s_1^{\alpha} = \frac{1 - Y_1(R_{ct} + R_S)}{(Y_1 R_S R_{ct} - R_{ct})Q_{dl}} \quad \text{and} \quad s_2^{\alpha} = \frac{1 - Y_2(R_{ct} + R_S)}{(Y_2 R_S R_{ct} - R_{ct})Q_{dl}}$$

After division of both equations:

$$\frac{s_1^{\alpha}}{s_2^{\alpha}} = \frac{\frac{1 - Y_1(R_{ct} + R_s)}{(Y_1 R_s R_{ct} - R_{ct})Q_{dl}}}{\frac{1 - Y_2(R_{ct} + R_s)}{(Y_2 R_s R_{ct} - R_{ct})Q_{dl}}} = \frac{\frac{1 - Y_1(R_{ct} + R_s)}{(Y_1 R_s R_{ct} - R_{ct})}}{\frac{1 - Y_2(R_{ct} + R_s)}{(Y_2 R_s R_{ct} - R_{ct})}} \tag{14}$$

and after logarithmizing

$$\ln s_1^{\alpha} - \ln s_2^{\alpha} = \alpha(\ln s_1 - \ln s_2) = \ln\left[\frac{1 - Y_1(R_{ct} + R_s)}{(Y_1 R_s R_{ct} - R_{ct})}\right] - \ln\left[\frac{1 - Y_2(R_{ct} + R_s)}{(Y_2 R_s R_{ct} - R_{ct})}\right] \quad (15)$$

α can be calculated.

$$\alpha = \frac{\ln\left[\frac{1 - Y_1(R_{ct} + R_s)}{(Y_1 R_s R_{ct} - R_{ct})}\right] - \ln\left[\frac{1 - Y_2(R_{ct} + R_s)}{(Y_2 R_s R_{ct} - R_{ct})}\right]}{(\ln s_1 - \ln s_2)} \quad (16)$$

Q_{dl} is found as:

$$Q_{dl} = \frac{\frac{1 - Y_1(R_{ct} + R_s)}{(Y_1 R_s R_{ct} - R_{ct})}}{s_1^{\alpha}} = \frac{1 - Y_1(R_{ct} + R_s)}{(Y_1 R_s R_{ct} - R_{ct}) s_1^{\alpha}} \quad (17)$$

3. Results and Discussion

3.1 Biofilm growth during 24 hours after 48 h incubation

The intention of the experiments was to show how a biofilm develops in the vicinity of an already established biofilm on 0.4 cm² gold electrodes. Therefore, each second electrode was inoculated, while all other electrodes were left blank. After incubation with separated reservoirs, the electrodes were transferred to the measurement chamber with only one reservoir for all electrodes. The impedance spectra, derived as described here, for different cell density during inoculation, are shown in Fig. 11. The highest impact of bacterial growth was found for the electrodes with the highest cell density (Fig. 11.C). The impedance at the blank electrodes increased as well due to migrating cells from the biofilm at the other electrodes spreading on the surface.

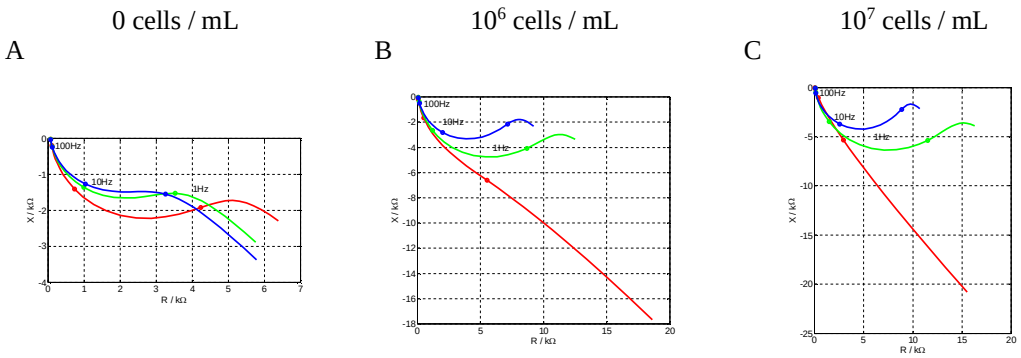

Figure 11. *Impedance spectra of a E-coli-biofilm calculated from current relaxation due to a voltage step of 32 mV. The inoculated electrodes have been incubated for 48 h in a special incubation chamber with individual compartments and for another 24 h in the measurement chamber where the impedance was measured immediately after transfer (blue), 2h after transfer (green) and again after 24 h (red). The dotted indicate frequency points that are labeled for all three curves together.*

The spectra in Fig. 11 are nice guidance, but they are not suitable for a quantitative explanation of the biofilm behavior. Since the Randles model is suitable for an explanation of behavior on the level of the electric double layer but also for the diffusive mass transport with the bulk of the biofilm, these model parameters are used for further interpretation.

4. Discussion

The blank electrodes show a surface capacitance of about 20 µF/cm² (fig. 12A), while an electrode with a densely packed cell monolayer reaches only less than 1 µF/cm² due to the membrane structures

with a typical capacity of 1 µF/cm². At the inoculated electrodes, a dense cell layer was found with lower capacitance for the electrodes with higher cell density (10^7 cells/mL) than those with fewer cells (10^6 cells/mL). After 2 hours, Q_{dl} increased slightly for all electrodes and reached the values for blank electrodes after 24 h. The Q_{dl} for the blank electrodes seems to increase as well but was not found to be significant. The charge transfer resistance at blank electrodes (fig.12C) is about 1.1 kΩcm² but increases due to the high resistance of cell membranes touching the electrode surface. With the degradation of the biofilm but also with the appearance of electron transfer centers, R_{ct} decreases again. Looking at Fig. 11C, the electrodes inoculated with 107 cell/mL showed the highest R_{ct}, which increased again during the first 2 h but decreased afterward dramatically below the initial level of 1.2 kΩcm². The other electrodes showed the same trend but with some delay, especially for the blank electrodes where the biofilm just started to grow, and only a few cells already spread at the electrode surface.

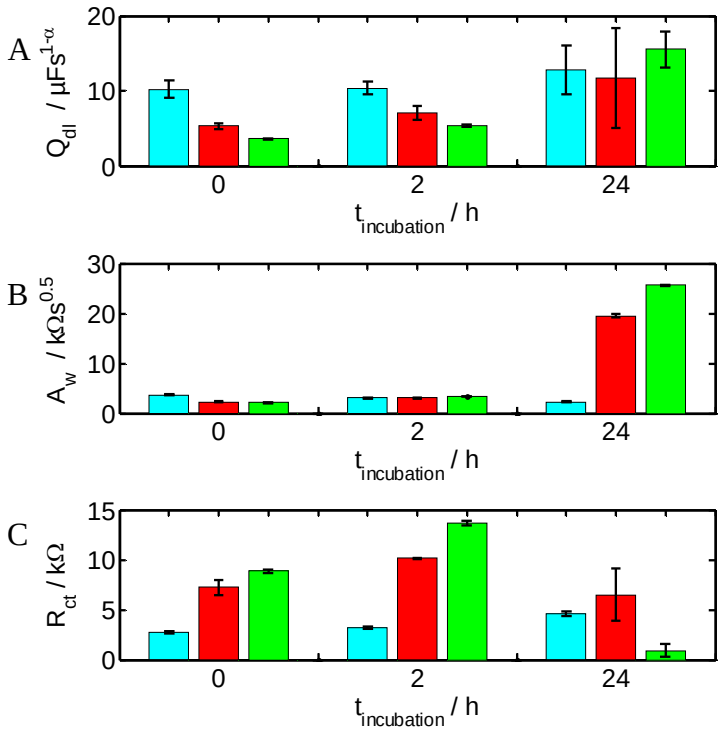

Figure 12. *(A) CPE-coefficient for double-layer capacitance Q_{dl}, B() Warburg coefficient A_W and (C) charge transfer resistance R_{ct} changing with time for different density of cells during inoculation*

While the surface capacitance (at first glance Q_{dl}) of the electrodes increases back to values of blank electrodes and R_{ct} decreases even to pre-growth values, the Warburg coefficient A_w increases dramatically within 24 h. This proves that the biofilm develops further instead of degrading. The high A_w is a hint to a biofilm with an increasing thickness, which is reflected by the increasing hindrance of charge carrier diffusion. This, however, appears away from the electrical double layer at the electrode where R_{ct} and Q_{dl} are determined by the electron exchange with electrodes reaching the electrode and the thickness of the layer with fixed charges.

Table 3. *Changes in α and the electrolyte resistance R_s*

	α	R_s / Ω
no inoculation	0.927 ± 0.003	74.08 ± 9.84
10^6 cell/mL	0.933 ± 0.020	85.26 ± 14.07
10^7 cell/mL	0.934 ± 0.015	71.54 ± 3.40

Differences in the distribution coefficient α turned out to be not significant. Although the saline resistance R_s was expected not to change, it showed some variance (tab.3).

The procedures presented here have been applied to data from growing bacterial biofilm in order to show the general applicability of relaxation measurements for electrical characterization. Although the calculation effort seems to be a major drawback, it is once programmed and executed by computers, thereby not realized by the operator of a device working on this basis.

The Laplace transformation, or for periodic signals the Fourier transformation, of the step response into the frequency domain was the standard procedure when equidistant sampling was used. Non-equidistant sampling can tremendously reduce the data volume and is favored for economic devices with low power requirements, minimal hardware, and narrow bandwidth for data transmission. The procedure for handling the *i(t)*- or *u(t)*-data is universal and generally applicable. However, the model in Eq. 2 is dedicated to a given MUT (modified Randles circuit) and should be adjusted depending on the measured data and the knowledge about the MUT. In practice, it is often not advisable to fit too much data, especially not, if they are not significant.

Compared to the direct impedance measurement in the frequency domain, a much higher effort for data processing seems to be unavoidable. However, the processing can be done after data transmission by a more powerful machine than the controller of a sensor. As shown here, the model parameters like charge transfer resistance or Warburg coefficient are directly obtained from fit to the relaxation curve in the time domain. Thus, the transformation of voltage or current into the frequency domain is unnecessary.

If in time domain only exponentials (also Mittag-Leffler-function) with discrete or distributed relaxations times are used, the calculated impedance spectrum is always fully Krames-Kronig conform.

5. Conclusions

Measurement and processing of electrical data in time domain yields exactly the same information as in frequency domain but avoids the complex nonlinear fit of impedance or admittance. Especially for process instrumentation, it is advantageous to extract the physical, chemical or biological behavior of interest directly from the relaxation (time constants, relaxation strength) and skip the rather complicate transformation into the impedance spectrum. However, once time constants and relaxation strengths are known, the impedance (or admittance) can be calculated analytically without Fourier or Laplace.

The electrical characterization of biofilms was shown here as an example. The interpretation of the model elements is not a feature of the measurement in the time domain but corresponds exactly to the model fit of the impedance spectrum measured in the frequency domain.

Acknowledgments

This work was partially supported by the Thüringer Aufbaubank (2016FGR0400) and AiF (FKz.4000403MD6). We thank Dieter Frense for critical review of the manuscript.

References

BioLogic. (2017). Distribution of Relaxation Times (DRT): an introduction. In BioLogic (Ed.), *https://www.biologic.net/documents/battery-eis-distribution-of-relaxation-times-drt-electrochemistry-application-note-60/* (Vol. #60). Seyssinet-Pariset, France.

Cole, R. H. (1955). On the Analysis of Dielectric Relaxation Measurements. *Journal of Chemical Physics, 23*(3), 493-499.

Gansauge, C., Zaikou, Y., Schroeder, V., Schemberg, J., & Pliquett, U. Fast Bio-Impedance Analysis using Electrical Relaxation.

Grimnes, S., & Martinsen, O. G. (2014). *Bioimpedance and Bioelectricity Basics*: Academic Press.

Haubold, H. J., Mathai, A. M., & Saxena, R. K. (2011). Mittag-Leffler functions and their applications. *Journal of Applied Mathematics, 2011*.

Horowitz, J. C., & Hill, F. R. (1980). *The Art of Electronics*. Cambridge, UK: Cambridge University Press.

Monje, C. A., Chen, Y., Vinagre, B. M., Xue, D., & Feliu, V. (2010). *Fractional-order Systems and Controls*. London: Springer.

Pliquett, U. (2018). Time Domain-Based Impedance Detection. *Capacitance Spectroscopy of Semiconductors*, 179.

Sadkowski, A. (2000). On the ideal polarisability of electrodes displaying cpe-type capacitance dispersion. *Journal of Electroanalytical Chemistry, 481*(2), 222-226.

Schwan, H. P. (1957). Electrical Properties of Tissue and Cell Suspensions. *Advances in Biophysics, 5*, 147-209.